BMC Cancer

RESEARCH Open Access

Role and molecular mechanisms of HuangQiSiJunZi decoction for treating triple-negative breast cancer as explored via network pharmacology and bioinformatics analyses

Decai Wang[1], Dongqing Xie[2†], Shuai Meng[3†], Jiwei MI[4], Haiming Wang[3], Lingsheng Li[3], Yin Zhang[3*] and Yixin Cui[3*]

Abstract

Objective In this study, we evaluated the molecular mechanisms of HuangQiSiJunZi Decoction (HQSJZD) for treating triple-negative breast cancer (TNBC) using network pharmacology and bioinformatics analyses.

Methods Effective chemical components together with action targets of HQSJZD were selected based on the Traditional Chinese Medicine Systems Pharmacology Database and Analysis Platform (TCMSP). Meanwhile, differentially expressed genes (DEGs) were extracted from TNBC sample data in The Cancer Genome Atlas (TCGA) database. Additionally, we built a protein-protein interaction (PPI) network and acquired hub genes. Gene Expression Omnibus(GEO) datasets were utilized to verify the accuracy of hub gene expression. Additionally, enrichment analyses were conducted on key genes. Furthermore, TNBC severity-related high-risk factors were screened through univariate together with multivariate Cox regressions; next, the logistic regression prediction model was built. Moreover, differential levels of 22 immune cell types in TNBC tissues compared with normal tissues were analyzed. The hub gene levels within pan-cancer and the human body were subsequently visualized and analyzed. Finally, quantitative PCR (RT-qPCR) was used to validate the correlation of the hub genes in TNBC cells.

Results The study predicted 256 targets of active ingredients and 1791 DEGs in TNBC, and obtained 16 hub genes against TNBC. The prognostic signature based on *FOS*, *MMP9*, and *PGR* was independent in predicting survival. A total of seven types of immune cells, such as CD4 + memory T cells, showed a significant difference in infiltration ($p < 0.05$), and immune cells were related to the hub genes. The HPA database was adopted for hub gene analyses, and as determined, *FOS* was highly expressed in most human organs. The results of RT-qPCR validation for the FOS hub gene were consistent with those of bioinformatic analyses.

†Dongqing Xie and Shuai Meng co-first author.

*Correspondence:
Yin Zhang
zhangyin@301hospital.com.cn
Yixin Cui
cuiyixin@301hospital.com.cn

Full list of author information is available at the end of the article

© The Author(s) 2024. **Open Access** This article is licensed under a Creative Commons Attribution-NonCommercial-NoDerivatives 4.0 International License, which permits any non-commercial use, sharing, distribution and reproduction in any medium or format, as long as you give appropriate credit to the original author(s) and the source, provide a link to the Creative Commons licence, and indicate if you modified the licensed material. You do not have permission under this licence to share adapted material derived from this article or parts of it. The images or other third party material in this article are included in the article's Creative Commons licence, unless indicated otherwise in a credit line to the material. If material is not included in the article's Creative Commons licence and your intended use is not permitted by statutory regulation or exceeds the permitted use, you will need to obtain permission directly from the copyright holder. To view a copy of this licence, visit http://creativecommons.org/licenses/by-nc-nd/4.0/.

Conclusion HQSJZD might regulate the interleukin-17 and aging pathways via *FOS* genes to increase immune cell infiltration in TNBC tissues, and thus, may treat TNBC and improve the prognosis. The *FOS* genes are likely to be a new marker for TNBC.

Keywords HuangQiSiJunZi decoction, Triple-negative breast cancer, Network pharmacology, Bioinformatics analyses, Medicinal herb

Introduction

There are more and more patients with breast cancer (BC) being diagnosed annually. According to the latest statistics in 2020, the newly diagnosed BC cases in the world reached 2,260,000, and the disease has become the most common cancer in women [1]. Triple-negative breast cancer (TNBC), a special BC subtype, is featured by the negative expression of the estrogen receptor (ER), the progesterone receptor (PR), and the human epithelial growth factor receptor 2 (Her2). TNBC accounts for 15–20% of BC cases in terms of morbidity, and it is more frequently seen in people carrying the BRCA gene mutations and in young African American women [2], with poorer prognosis in younger patients [3]. TNBC is not responsive to endocrine therapy or HER2 inhibitors; therefore, surgery, chemotherapy, and radiotherapy are the major treatments for the disease. Typically, TNBC is characterized by its high invasiveness, distant metastasis rate, local relapse risk, and heterogeneity [4–6]. The chemoresistance rate is relatively high and the patient prognosis is dismal. Approximately 25–30% of patients with early TNBC develop distant metastases within 3–5 years, even after the primary lesions are successfully treated, and this risk exists for a long time [7, 8], which is an important issue currently encountered by clinical physicians [9]. Consequently, it is of crucial importance to devise treatment options for improving the prognosis of TNBC patients.

Till date, the traditional Chinese medicine (TCM) treatment of TNBC has achieved great success. TCM could improve the quality of life, prolong the progression-free survival (PFS) of tumor patients, and prevent disease exacerbation. According to the TCM theory, TNBC is associated with vital qi deficiency, which is an important fundamental and decisive factor for the pathogenesis and development of TNBC [10]. Because of the vital qi deficiency, the toxin is likely to relapse or migrate to other sites, resulting in malignant biological behaviors such as proliferation, invasion, and migration. In this regard, invigorating qi and strengthening the body resistance is an effective method to treat TNBC.HuangQiSiJunZi Decoction(HQSJZD)is comprised by Astragalus along with the classical SiJunZi Decoction for replenishing qi to invigorate the spleen. The SiJunZi Decoction contains Ginseng, Rhizoma Atractylodis, Poria cocos, and Glycyrrhiza, which exert the therapeutic effect through replenishing qi to invigorate the spleen. Notably, the addition of Astragalus could further enhance its activities of tonifying qi to invigorate the spleen and support healthy energy. Modern pharmacological research has revealed that Astragalus polysaccharides (APS) could participate in the mitochondrial apoptotic pathway of BC cells, promote cell apoptosis of cells in BC tissue, and thus inhibit tumor cell growth [10]. The SiJunZi Decoction can improve complications after chemotherapy and surgery for BC, induce TNBC cell apoptosis, suppress TNBC cell proliferation, and significantly improve the patients' quality of life [11]. HQSJZD may induce an increase in the numbers of CD3+CD4+T and CD3+CD8+T cells within the tumor microenvironment (TME), recover the innate immunity of the body, and enhance the surveillance function of the immune system. Moreover, HQSJZD is involved in the inflammatory response, induces cancer cell apoptosis, and thereby suppresses the proliferation and migration of malignant cancer cells [12–14]. HQSJZD has been used in the clinical treatment of the malignant tumors and has achieved favorable effects [15, 16].Clinical observations have discovered that HQSJZD can significantly improve the adverse reactions of BC patients during chemotherapy and has a certain regulatory effect on immunity [17], however, its therapeutic effect on TNBC remains largely unexplored. Therefore, it is necessary to construct a systemic research strategy to comprehensively illustrate its molecular mechanisms, and thereby, lay a theoretical basis and scientific foundation for its clinical application. In this regard, this study aimed to fill this gap by exploring the specific mechanisms of HQSJZD in treating TNBC, so as to provide a scientific basis for its potential in clinical application.

Methods

This study focused on investigating the possible targets and pharmacological mechanisms underlying the multiple active ingredients of HQSJZD against TNBC through a network pharmacophore model and bioinformatics analyses. In the study, we acquired a least absolute shrinkage and selection operator (LASSO)-Cox prognostic regression model. Furthermore, we conducted gene set enrichment analysis (GSEA) for investigating the impacts of model core genes on the immune response. Additionally, associations of risk scores with immune cells were analyzed. The molecular mechanisms related to HQSJZD in treating TNBC were investigated to provide evidence for its role in the treatment and provide

new information to apply TCM in tumor treatment. (Fig. 1).

Collection and selection of active ingredients along with targets of HQSJZD

Information on the components of five herbal medicines in HQSJZD was obtained from the TCMSP database (https://tcmspw.com/tcmsp.php) [18] by using the terms "Rhizoma Atractylodis", "Ginseng", "Poria cocos" and "Glycyrrhiza," with a drug likeness (DL) ≥ 0.18 and an oral bioavailability (OB) ≥ 30% being used as standards. Thereafter, species in the UniProtKB database (https://www.uniprot.org/; date of retrieval, February 10, 2023) were restricted to "Homo sapiens", and the corresponding genes of the targets were identified.

Breast cancer data

For this study, we obtained the BC dataset (TCGA-BRCA) based on The Cancer Genome Atlas (TCGA; https://portal.gdc.cancer.gov/) by adopting TCGA biolinks package [19]. Subsequently, TNBC samples with negative ER, PR, and human epidermal growth factor receptor-2 (Her-2) levels detected through immunohistochemistry were selected to obtain 127 TNBC samples with available clinical information, including the count sequencing data of 116 tumor tissues from patients with TNBC (TNBC group) and 11 para-carcinoma normal tissues (Normal group). All data were normalized into the Transcripts Per Million (TPM) format, while relevant clinical data were acquired based on the UCSC Xena database (http://genome.ucsc.edu) [20]. TCGA dataset was selected as the test set. The TNBC-related datasets GSE38959 [21], GSE76274 [22], and GSE76124 [22] were downloaded from the GEO database using the GEOquery [23] package, and all datasets corresponding to *Homo sapiens* were obtained. We obtained the GSE38959 dataset from the GPL4133 data platform, which included 47 samples, and among which, 30 mammary duct cell samples from TNBC group and 13 normal mammary duct cell samples from the Normal group were selected for the analyses. The GSE76274 dataset was obtained from the GPL570 data platform, which included 67 samples, all of which were incorporated into the analyses. The GSE76124 dataset was obtained from the GPL570 data platform, which included 198 samples, of which 67 TNBC mammary tissue samples were selected for the analyses. The three GEO datasets were merged as the verification set.

DEGs in TNBC

For identifying common differentially expressed genes (DEGs) in TNBC, TCGA-TNBC expression profiles were differentially analyzed using the limma package, with thresholds of |logFC| >2 and p.adjust < 0.05. Specifically,

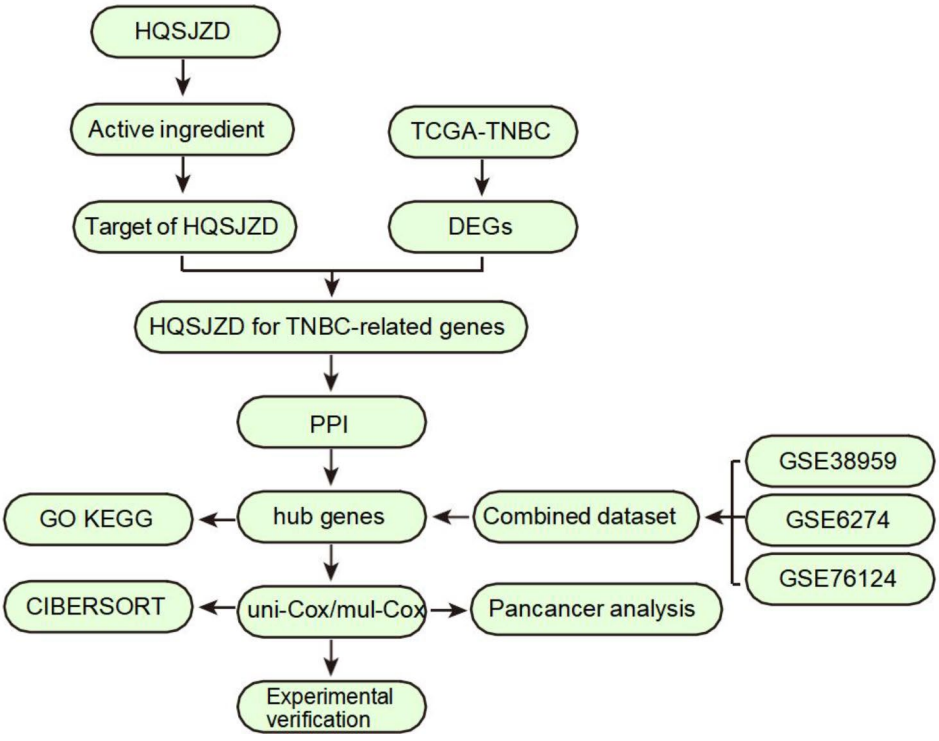

Fig. 1 A flow chart of the research strategy. HQSJZD: HuangQiSiJunZi Decoction; TNBC: Triple Negative Breast Cancer; DEGs: Differentially expressed genes; PPI: Protein-protein interaction; GO: Gene Ontology; KEGG: Kyoto Encyclopedia of Genes and Genomes

DEGs with logFC > 2 and p.adjust < 0.05 were considered to be upregulated, whereas those with logFC < −2 and p.adjust < 0.05 were considered to be downregulated.

Genes related to the effect of HQSJZD on TNBC

The screened target proteins of TCM components and the identified DEGs were intersected to obtain the target proteins for HQSJZD for TNBC-related genes, following which a Venn diagram was plotted. Additionally, the TCM-component-target information network diagram was visualized. Next, a heatmap and volcano plot of TCGA-TNBC dataset were drawn based on the obtained HQSJZD targets for the TNBC-related genes.

Protein-protein interaction (PPI) network

In this study, we used the STRING database [24] to construct a PPI network of HQSJZD for TNBC-related genes based on the threshold of a minimum correlation coefficient > 0.400, with the species being limited to *Homo sapiens*. Additionally, Cytoscape was adopted for visualizing PPI network model construction [25]. Furthermore, five algorithms in the cytoHubba plug-in [26], including Degree (Degree Correlation), MNC (Maximum Neighborhood Component), MCC (Maximal Clique Centrality), EPC (Edge Percolated Component), and Closeness (Closeness Centrality), were used to calculate the scores. Finally, the 20 most significant genes acquired by these five algorithms were overlapped to obtain the hub genes.

Gene Ontology (GO) and Kyoto Encyclopedia of genes and genomes (KEGG) analyses of the hub genes

The hub genes were subjected to GO analyses. Generally, GO terms are classified into biological process (BP), cell component (CC), and molecular function (MF) categories [27]. By using the R package clusterProfiler [28], the hub genes were subjected to GO annotation analyses, and the items were selected based on the criteria of p.adjust < 0.05 and FDR (q.value) < 0.25, whereas the P-value was adjusted using the Benjamini-Hochberg (BH) approach. Finally, the R package Pathview [29] was employed for KEGG pathway enrichment [30] to visualize the related pathways.

Verification of expression of the hub genes

The R package sva [31] was used to subject the GSE38959, GSE76274, and GSE76124 datasets to batch removal (Supplementary Figure S1) to obtain the combined dataset. To verify the expression of the hub genes, we applied a Wilcoxon rank sum test when plotting a group comparison diagram of the hub genes among different groups of TCGA-TNBC datasets and the combined dataset (TNBC and Normal). Subsequently, genes with a significant differential expression were screened to draw receiver operating characteristic (ROC) curves for diverse datasets.

Performance of the hub genes-based prognostic model in prognosis prediction

The hub gene levels were analyzed with a univariate Cox regression, with genes of $p < 0.1$ being further selected for subsequent analyses. Thereafter, we plotted time-dependent ROC curves for displaying influences of hub genes on 1-, 3-, and 5-year survival outcomes. Later, a multivariate Cox regression was conducted on TCGA-TNBC dataset to explore the correlations between expression of hub genes and stage as well as clinical prognosis of TNBC, which was followed by construction of the multivariate Cox regression model. Subsequently, in line with the multivariate Cox regression results, a nomogram was constructed using the R package rms [32]. A certain scale was set to assign scores to various variables in the multivariate regression model. Subsequently, a total score was calculated to predict the event occurrence probability. Finally, the nomogram accuracy and resolution were evaluated by a calibration curve. A calibration graph [33] can judge the model prediction efficiency according to real results by fitting real measurement data to the model predicted probability in diverse situations in the graph. This method could be adopted when fitting a Cox regression constructed model to a real measurement data. Decision curve analysis (DCA) [34] is an easy approach to evaluate the clinical prediction model, diagnostic test, and molecular markers. We adopted a DCA diagram to evaluate the Cox regression model resolution and prediction performance. In addition, the DCA diagram was plotted with the R package ggDCA [35] to evaluate the Cox regression model performance. The formula for the multivariate Cox model is shown below:

$$\mathrm{Risk}Score = \sum {}_i\beta \, {}_iS_i$$

βi = the regression coefficient for the gene; *Si* = the correlation score for the gene.

Immune infiltration analyses

CIBERSORT (https://cibersort.stanford.edu/) [36] is a web-based tool applied to the deconvolution of human immune cell subtype expression matrix according to the linear support vector regression principle. CIBERSORT can evaluate the infiltrating degrees of immune cells within the sequenced samples in line with the gene expression feature set in the known 22 immune cell subtypes. We utilized the CIBERSORT algorithm to evaluate the infiltrating levels of immune cells in the combined dataset, while correlations among the different immune cells were determined by Spearman's correlation analysis, which was further carried out for determining the correlations between the hub genes and tumor-infiltrating immune cells (TIICs) in the TME. The heat map and

lollipop diagram were drawn and visualized with the R package "ggplot2".

Pan-cancer analyses of hub genes

RNAseq data of 33 cancers, which were in TPM format and processed by the STAR procedure, were obtained from TCGA database and transformed into log2 values to analyze and compare the different levels of the prognosis-related hub genes within the samples. Furthermore, we adopted the Human Protein Atlas (HPA) database (www.proteinatlas.org/) [37] to analyze the prognosis-related hub gene levels in human organs.

Real-time quantitative polymerase chain reaction (RT-qPCR)

To measure the gene expression of *EGF*, *FOS*, *PGR*, *IGF2*, *SPP1*, *MMP1*, and *PPARG*, MDA-MB-468 human BC cells (Saibaikang), MDA-MB-157 human BC cells (Saibaikang), and MCF-10 A human breast epithelial cells (Saibaikang) were cultured in normal medium (final glucose concentration of 5.5 mM) and high glucose medium (final glucose concentration of 30 mM) for 48 h [38]. Total RNA was extracted using the TRIzol reagent (Invitrogen, 15596-018,CA, USA) and the RNA solution was diluted 20X. The RNA concentration was detected and calculated using a spectrophotometer(Thermo Fisher Scientific, USA, NanoDrop2000). The RNA was then reverse transcribed into cDNA using the All-in-One SuperMix kit (TransScript), and the obtained cDNA was stored at −20℃ or below. The cDNA samples were diluted 10X and used as templates for the RT-qPCR reaction, which was performed in a 96-well plate on an ABI quantstudio5 fluorescence quantitative PCR instrument. Each experiment was repeated three times. The polymerase chain reaction (PCR) conditions were as follows: 95℃ × 5 min for pre-denaturation (1 cycle); followed by denaturation at 95℃ × 10 s and annealing/extension at 60℃×30 s for 40 cycles. The primer sequences are listed in Supplementary Table 1; the primers were synthesized by Sangon Biotech (Shanghai, China). After the PCR, the data were analyzed using the 2-ΔΔCt method [38]. (Table 1).

Table 1 Sequences of the primers for RT-qPCR

Primer name	Forward primer (5′→3′)	Reverse primer (5′→3′)	Size of amplified of products (bp)
H-GAPDH	GGAGCGAGATCCCTCCAAAAT	GGCTGTTGTCATACTTCTCATGG	197
H-EGF	TGTCCACGCAATGTGTCTGAA	CATTATCGGGTGAGGAACAACC	133
H-FOS	GGGGCAAGGTGGAACAGTTAT	CCGCTTGGAGTGTATCAGTCA	126
H-PGR-1	GTCGAGCTCACAGCGTTTCT	TGCCCGGGACTGGATAAATG	109
H-PGR-2	CTCCATTGACTCGAACGACTC	CAGGTCTGCGAAACTTCTTAGAT	230
H-IGF2-F	GTGGCATCGTTGAGGAGTG	CACGTCCCTCTCGGACTTG	92
H-SPP1-1	GAAGTTTCGCAGACCTGACAT	GTATGCACCATTCAACTCCTCG	91
H-SPP1-2	TTATGGTGTCCTTACCTGTGGG	GCGGATTTTATCAACGATGCAG	112
H-MMP1	AAAATTACACGCCAGATTTGCC	GGTGTGACATTACTCCAGAGTTG	82
H-PPARG	TACTGTCGGTTTCAGAAATGCC	GTCAGCGGACTCTGGATTCAG	141

Statistical analyses

Data were processed and analyzed using R software (https://www.r-project.org/,Version 4.2.0,The R software is developed and maintained by the R Core Team). For comparison of continuous variables between two groups, normally distributed variables were examined for their statistical significance using the independent Student's t-test, while non-normally distributed data were analyzed using the Mann-Whitney U test (namely, the Wilcoxon rank-sum test). The Kruskal-Wallis test was used to compare several groups. Significant differences between categorical variables were compared using the Fisher exact test or the chi-square test. Results of correlation coefficients among diverse molecules were determined by Spearman's correlation analysis, and survival analysis was conducted using R package survival. Unless otherwise noted, all P-values were two-sided, and $p<0.05$ indicated that the difference was statistically significant.

Results

Screening of Chinese herbal compound molecules

Compound components of HQSJZD were acquired from the TCMSP database. Thereafter, effective compounds with an OB≥30% and a DL≥0.18 were screened, including 20 in Astragalus, 22 in Ginseng, 29 in Rhizoma Atractylodis, 15 in Poria cocos, and 92 in Glycyrrhiza. After deleting duplicate compounds, 145 active compounds were obtained, as shown in Table S1. We also utilized the TCMSP database to predict the protein targets corresponding with the active ingredients in Astragalus, Genseng, Rhizoma Atractylodis, Poria cocos, and Glycyrrhiza, which were transformed into gene names using UniProtKB to obtain 256 targets of the active ingredients in the Chinese herbal compound (Table S2). Figure 2 shows the TCM-component-predicted target network diagram.

TNBC-related DEG analyses

Differential analyses was conducted on TCGA-TNBC dataset using the limma package to obtain the DEGs, followed by the creation of a volcano plot (Fig. 3A). In

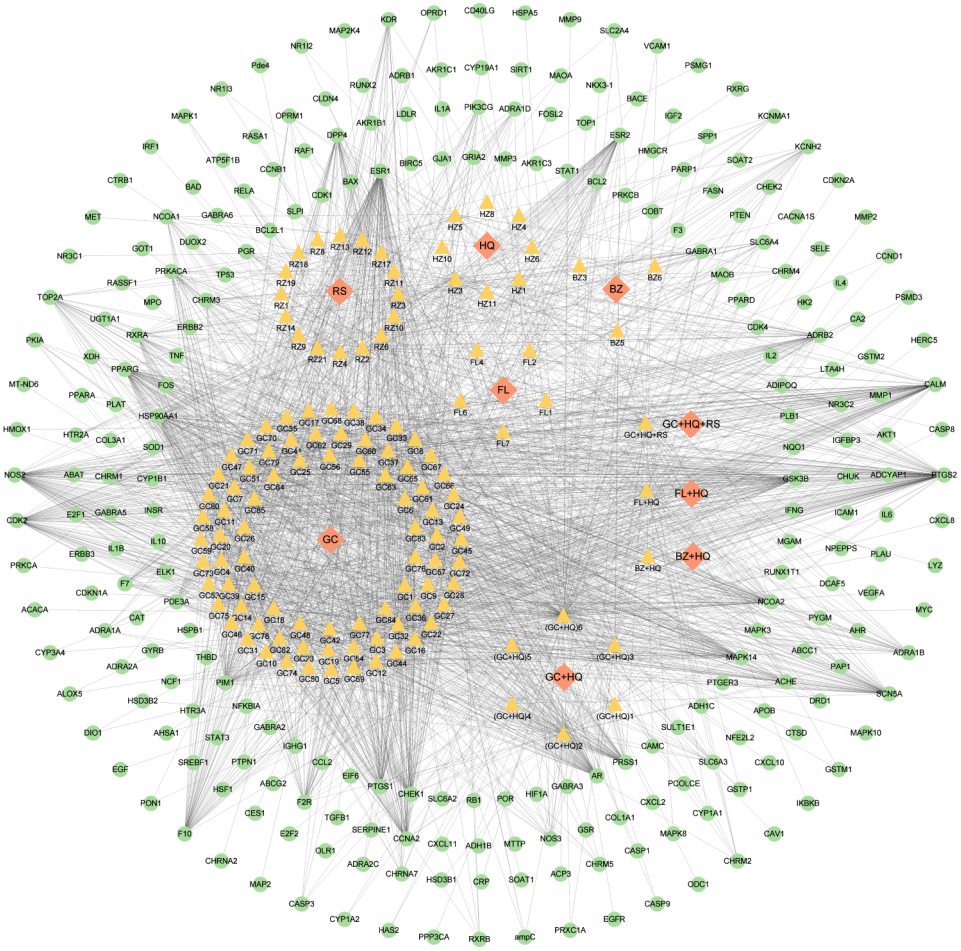

Fig. 2 Traditional Chinese medicine (TCM) -component-predicted target network diagram. The pink diamond, yellow triangle, and green dot represent the TCM, component, and target, respectively. HQ: Huangqi; FL: Fuling; GC: Gancao; BZ: Baizhu; GC: Gancao

TCGA-TNBC dataset, there were 1791 genes that satisfied |logFC| > 2 and P.adjust < 0.05. Under these thresholds, 795 DEGs were highly expressed in the TNBC group (lowly expressed within the Normal group; the logFC was positive; these were identified as the upregulated genes), whereas 996 DEGs were lowly expressed in the TNBC group (highly expressed in the Normal group; logFC was negative; these were the downregulated genes). The DEGs obtained from TCGA-TNBC dataset were intersected with the targets of the active ingredients in the Chinese herbal compound to obtain 58 HQSJZD for the TNBC-related genes. The Venn diagram (Fig. 3B) and heat map (Fig. 3C) were plotted.

PPI network

Using the STRING database, 58 HQSJZD for the TNBC-related genes were used for the PPI analyses, followed by construction and visualization of the PPIs via a PPI network using Cytoscape software (Fig. 4A). Thereafter, five algorithms, namely, MCC, MNC, EPC, Degree and Closeness, were analyzed using the cytoHubba plug-in, and the top 20 gene–gene interaction network diagrams obtained by the five algorithms after ranking were plotted (Fig. 4B-F). As shown in Table 2, their intersections were considered as the hub genes (mRNA) (*ESR1*, *CDKN2A*, *CCNA2*, *CCNB1*, *EGF*, *FOS*, *MMP9*, *AR*, *CDK1*, *PGR*, *BIRC5*, *IL6*, *IGF2*, *SPP1*, *MMP1*, and *PPARG*) (Fig. 4G).

GO and KEGG analyses of the hub genes

To analyze the levels of the 16 *FOS* hub genes in the BP, MF, and CC categories, we first conducted GO and KEGG analyses on the hub genes. GO annotation, together with KEGG pathway enrichment analyses results, are displayed in the histogram (Fig. 5A-D), as shown in Table S3.

As observed in Fig. 5A-D, the hub genes were mainly enriched in the BP category, such as epithelial cell proliferation, pregnancy, multi-multicellular organism process, multi-organism reproductive process, response to steroid hormone, regulation of protein serine/threonine kinase activity, gland development, reproductive structure development, gland morphogenesis, and mammary

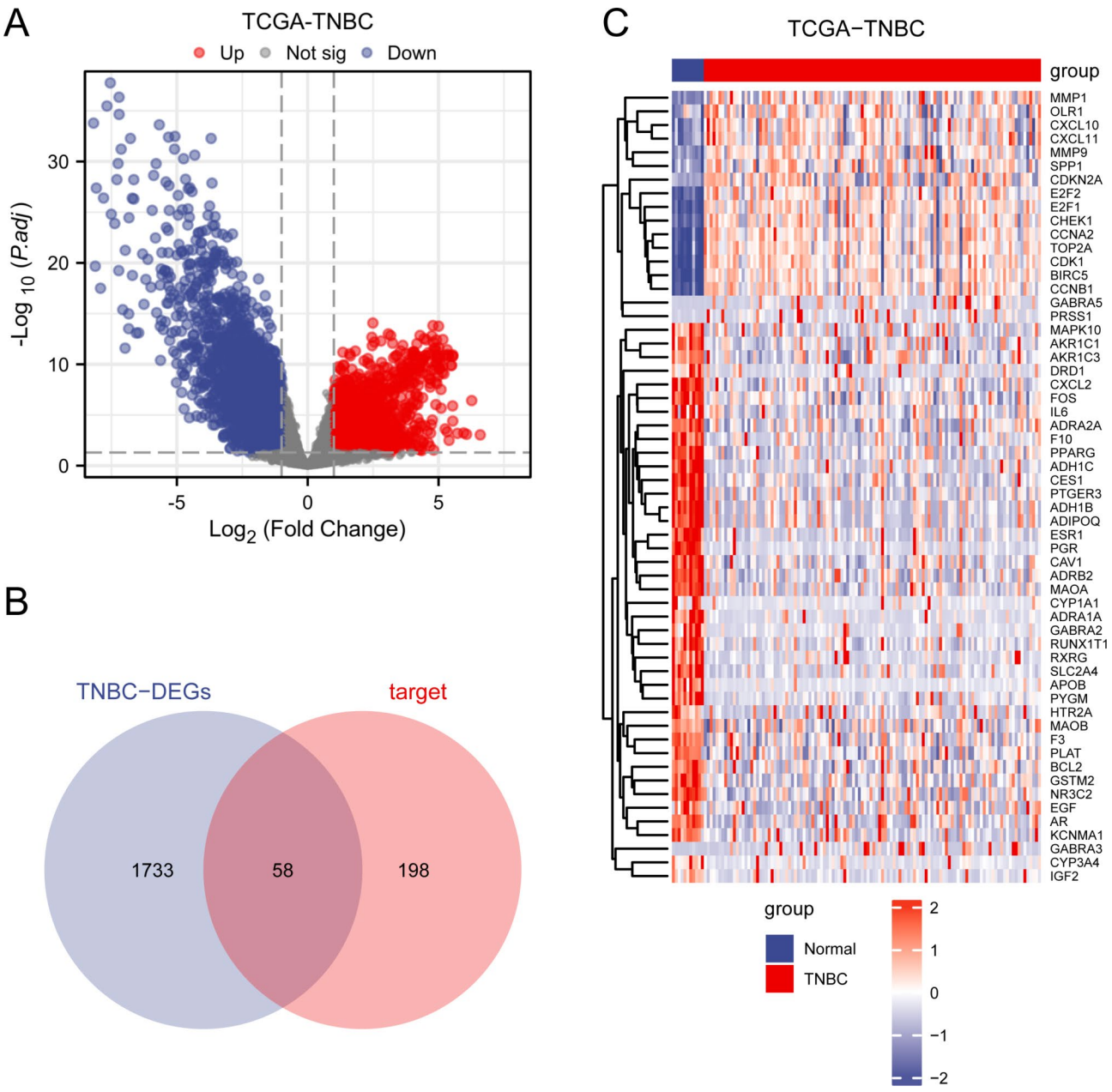

Fig. 3 TNBC-related DEGs analyses. (**A**) Volcano plot showing the DEGs between the TNBC and Normal groups in TCGA-TNBC dataset. (**B**) Venn diagram showing the DEGs and targets of TNBC. (**C**) Heatmap showing the DEGs and targets in TNBC.Heatmap showing HQSJZD targets for the TNBC-related genes in the TNBC and Normal groups in TCGA-TNBC dataset. HQSJZD: HuangQiSiJunZi Decoction; TNBC: Triple Negative Breast Cancer; DEGs: Differentially expressed genes

gland development. The CC terms enriched included the serine/threonine protein kinase complex, cyclin-dependent protein kinase holoenzyme complex, transferase complex, protein kinase complex, chromosomal region, transferring phosphorus-containing groups, spindle, transcription regulator complex, platelet alpha granule lumen, spindle microtubule, and platelet alpha granule. The MF terms enriched were transcription coregulator binding, protein kinase regulator activity, RNA polymerase II-specific DNA-binding transcription factor binding, kinase regulator activity, DNA-binding transcription factor binding, nuclear receptor activity, ligand-activated transcription factor activity, RNA polymerase II-specific, DNA-binding transcription activator activity, DNA-binding transcription activator activity, and receptor ligand activity. Additionally, the hub genes were mainly enriched into pathways such as chemical carcinogenesis-receptor activation, cellular senescence, lipid and atherosclerosis, IL-17 pathway, endocrine resistance, cell cycle, progesterone-mediated oocyte maturation,

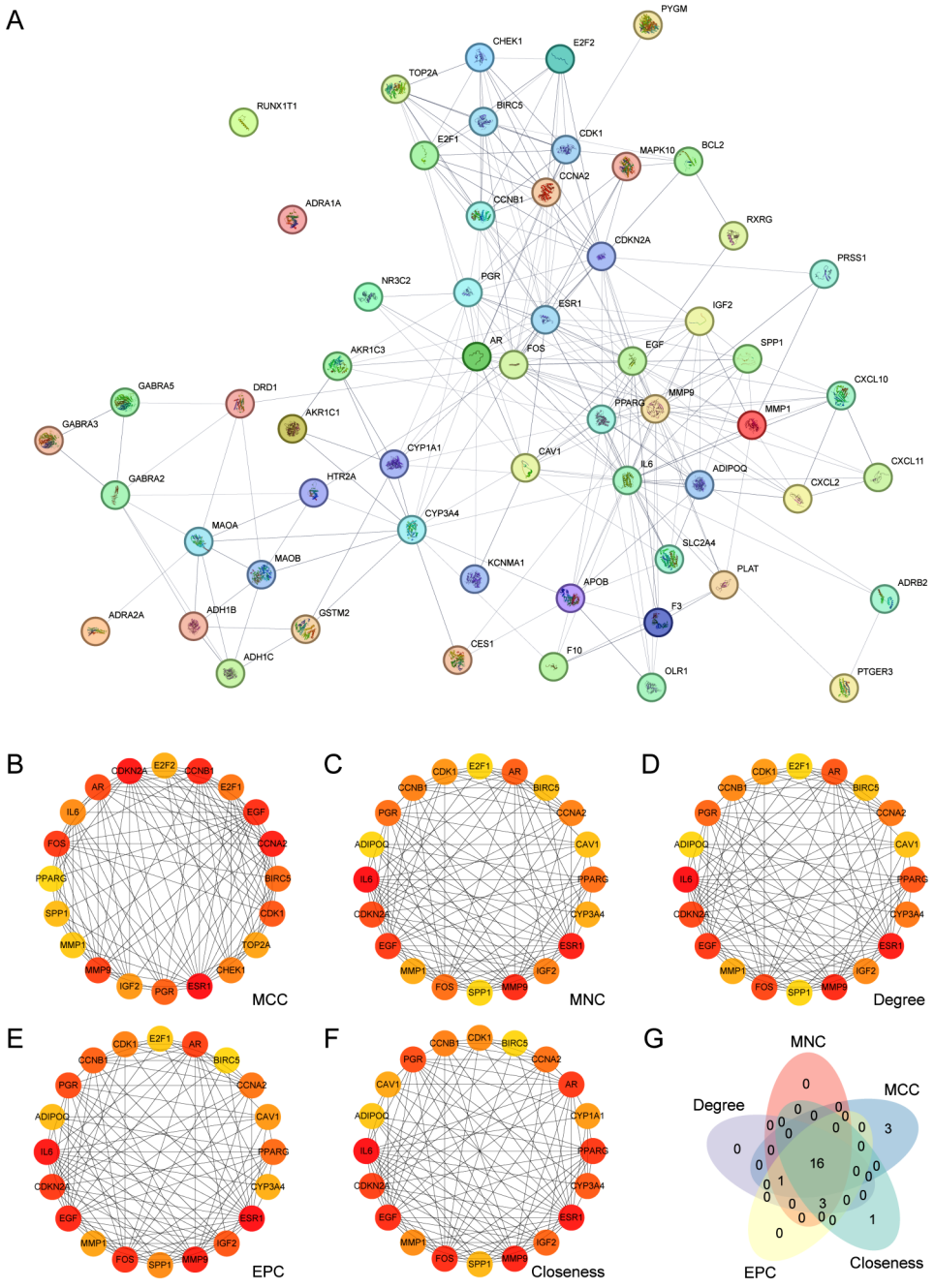

Fig. 4 PPI network. (**A**) PPI network of HQSJZD for the TNBC-related genes. (**B**-**F**) PPI networks of the five algorithms, namely, MCC (**B**), MNC (**C**), Degree (**D**), EPC (**E**), and Closeness (**F**). (**G**) Venn diagram revealing the intersections among the 20 most significant genes using the five algorithms. In B-F, higher scores are denoted by a darker color. HQSJZD: HuangQiSiJunZi Decoction; PPI network: Protein-protein interaction; Degree: Degree Correlation; MNC: Maximum Neighborhood Component; MCC: Maximal Clique Centrality; EPC: Edge Percolated Component; Closeness: Closeness Centrality

estrogen signaling pathway, oocyte meiosis, and breast cancer pathways. We chose to display two pathways: the IL-17 signaling pathway (Fig. 6A) and the breast cancer pathway (Fig. 6B).

Verification of hub gene expression

By applying the Wilcoxon rank sum test, the comparison diagrams of the hub genes among the diverse groups of TCGA-TNBC and combined GEO datasets (TNBC and Normal) were drawn (Fig. 7A-B). The results showed that *AR*, *BIRC*, *CCNA2*, *CCNB1*, *CDKN2A*, *ESR1*, *MMP1*, *PGR*, and *SPP1* exhibited significant differential expression between the two datasets ($p<0.01$), and the expression trends were consistent. The above-mentioned genes were used to plot ROC curves of different datasets (Fig. 7C-V). In TCGA-TNBC dataset, *AR*, *BIRC*,

Table 2 Analyses of topological parameters of hub genes

hub genes	MCC	MNC	Degree	EPC	Closeness
MMP1	5546	12	12	13.226	31
BIRC5	81,366	11	11	11.994	29
CDK1	87,126	13	13	13.619	31
CDKN2A	168,626	19	19	16.398	35
FOS	93,026	17	19	16.909	36
CCNA2	127,561	14	15	14.742	32.33333
CCNB1	127,560	14	14	15.085	31.83333
AR	87,386	18	18	16.343	35.25
PGR	81,768	17	17	16.093	34.75
ESR1	174,800	26	26	17.976	39.41667
IGF2	48,384	14	14	15.612	32.33333
IL6	50,250	27	27	17.686	39.75
SPP1	7440	10	10	13.543	30.16667
MMP9	90,185	22	23	17.21	37
PPARG	2577	17	18	15.045	35.25
EGF	95,112	21	21	16.996	36

CCNA2, *CCNB1*, *ESR1*, *MMP1*, *PGR*, and *PPARG* had relatively high accuracy in diagnosis (AUC > 0.9); whereas *CDKN2A* and *SPP1* were partially accurate in diagnosis (0.7 < AUC < 0.9). In the GEO dataset, *AR*, *BIRC*, *CCNA2*, *CCNB1*, *CDKN2A*, *ESR1*, *MMP1*, *PGR*, *PPARG*, and *SPP1* had moderately accurate diagnostic value (0.7 < AUC < 0.9).

Prognosis value of the hub genes

The hub gene levels from TCGA-TNBC dataset were incorporated into a univariate Cox regression analysis, and a forest map (Fig. 8A) was plotted. *FOS*, *MMP9*, and *PGR* were potential genes highly related to survival, which were of prognostic significance ($p < 0.1$). The time-dependent ROC curves of *FOS* (Fig. 8B), *MMP9* (Fig. 8C), and *PGR* (Fig. 8D) were plotted. The results showed that *FOS* had certain accurate prognostic significance at 1- and 3-year (0.7 < AUC < 0.9).

For TCGA-TNBC dataset, a multivariate Cox regression was used to determine correlations of the three prognosis-related hub genes (*FOS*, *MMP9*, and *PGR*) with stage and clinical prognosis for the TNBC cases, and a multivariate Cox regression model was constructed. The forest map was plotted to display the multivariate Cox regression results (Fig. 9A), as shown in Table 3. *FOS*, *MMP9*, and *PGR* were the prognosis-related genes for TNBC, and their HRs were > 1, indicating that they were the risk prognostic genes, with a more advanced stage indicating poorer clinical prognosis.

Nomogram analysis was also conducted to judge the model prognosis prediction ability, and a nomogram (Fig. 8B) was drawn. Calibration analyses were conducted on the nomograms of univariate, together with multivariate, Cox regression models on 1-, 3-, and 5-year survivals (Fig. 9C-E), and a calibration curve was determined. According to the results, the prognosis prediction model had the best effect on predicting 1- and 3-year survivals.

Thereafter, we applied DCA to evaluate the effect of the constructed Cox regression prognostic model to predict 1-, 3-, and 5-year survivals (Fig. 9F-H). The results showed that the performance of the constructed Cox regression prognostic model in predicting prognosis followed the order of 5-year > 3-year > 1-year, and it was of certain clinical application value.

Immune infiltration analyses of TCGA-TNBC dataset (CIBERSORT)

By adopting the CIBERSORT algorithm, 22 TIIC proportions were calculated according to TCGA-TNBC dataset, and the TIIC proportion diagram for the TNBC group and Normal group in the dataset was plotted (Fig. 10A). In addition, the immune cell proportion comparison diagram for the TNBC and Normal groups was drawn according to the differences in the TIIC infiltration degrees (Fig. 10B). Of these, the proportions of follicular helper T cells, CD4+memory activated T cells, regulatory T cells (Tregs), and macrophages M0 and M1 groups in the TNBC group increased compared with those of the Normal group ($P < 0.05$, Wilcoxon test). Further, the proportions of CD4+memory resting T cells and macrophages M2 from the TNBC group decreased compared to those of the Normal group ($P < 0.05$, Wilcoxon test). A heat map showing the correlations among the above-mentioned seven immune cells (Fig. 10C) and a heat map displaying the associations of immune cells with the hub genes (*FOS*, *MMP9*, and *PGR*) (Fig. 10D) were drawn. As observed from the figure, *MMP9* had the highest positive correlation with macrophages M0, while *MMP9* displayed an extremely high positive correlation with Tregs, and *PGR* had high positive correlation with CD4+memory resting T cells.

Hub gene expression in pan-cancer and in the human body

RNAseq data of 33 cancers, which were in TPM format, and were processed by the STAR procedure, were obtained from TCGA database and transformed into log2 values to analyze and compare the different levels of prognostic hub genes (*FOS*, *MMP9*, and *PGR)* in the samples (Fig. 11A-C). As observed in the figure, *FOS* was significantly differentially expressed in 16 cancers ($p < 0.05$), *MMP9* was significantly differentially expressed in 18 cancers ($p < 0.05$), and PGR was significantly differentially expressed in 16 cancers ($p < 0.05$). Moreover, the expression of prognosis-related *FOS* (Fig. 11D), *MMP9* (Fig. 11E), and *PGR* (Fig. 11F) in various human organs was verified based on the HPA database. As observed in the Fig. 11D, only *FOS* was expressed in the majority of the human organs.

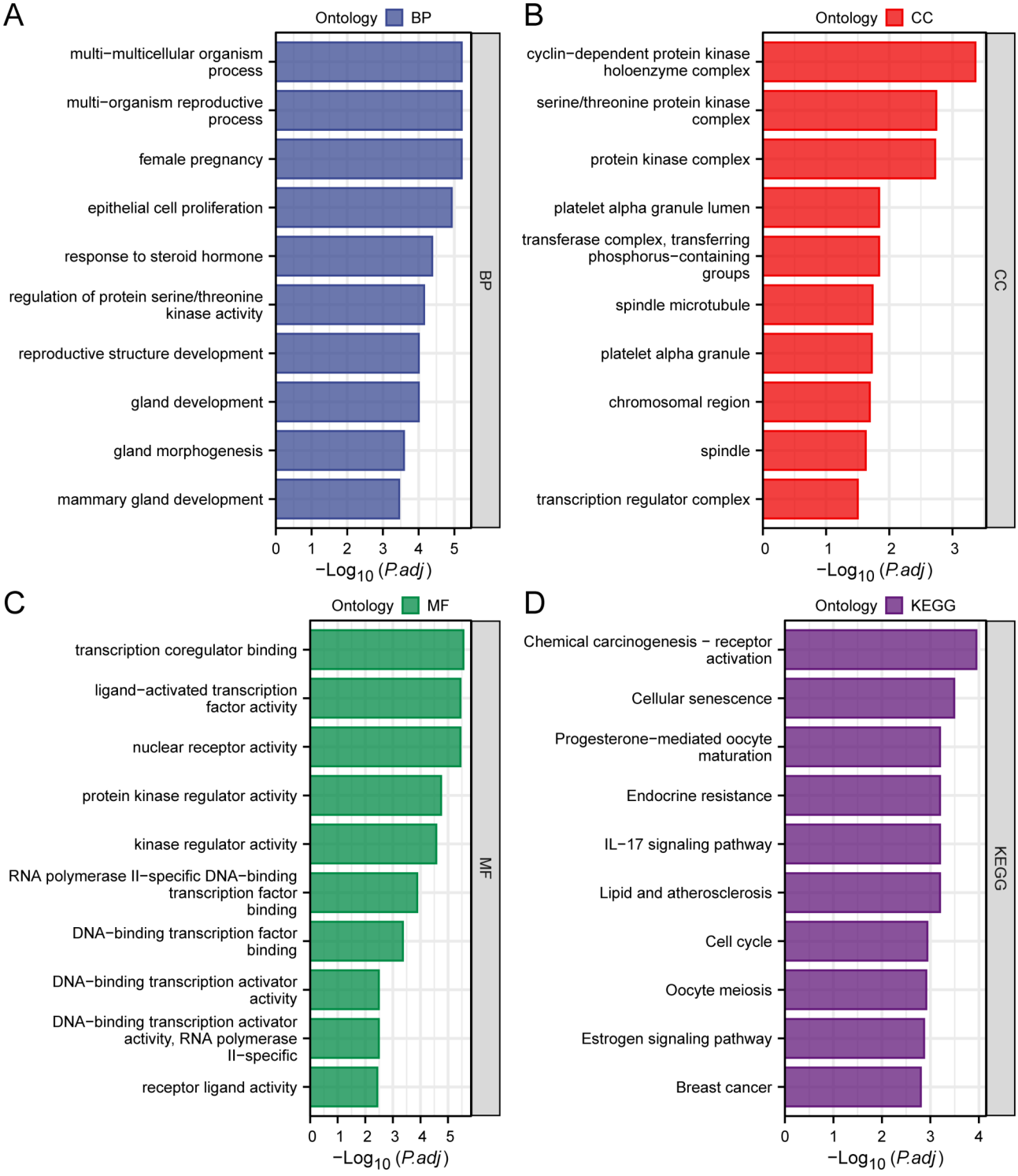

Fig. 5 GO annotation and KEGG analyses of the hub genes. (**A**-**C**). Histograms showing the BP, CC, and MF terms, respectively, enriched by the hub genes during GO functional annotation. (**D**) Histogram showing results of the KEGG enrichment analyses of the hub genes. GO: Gene Ontology; BP: biological process; CC: cellular component; MF: molecular function; KEGG: Kyoto Encyclopedia of Genes and Genomes

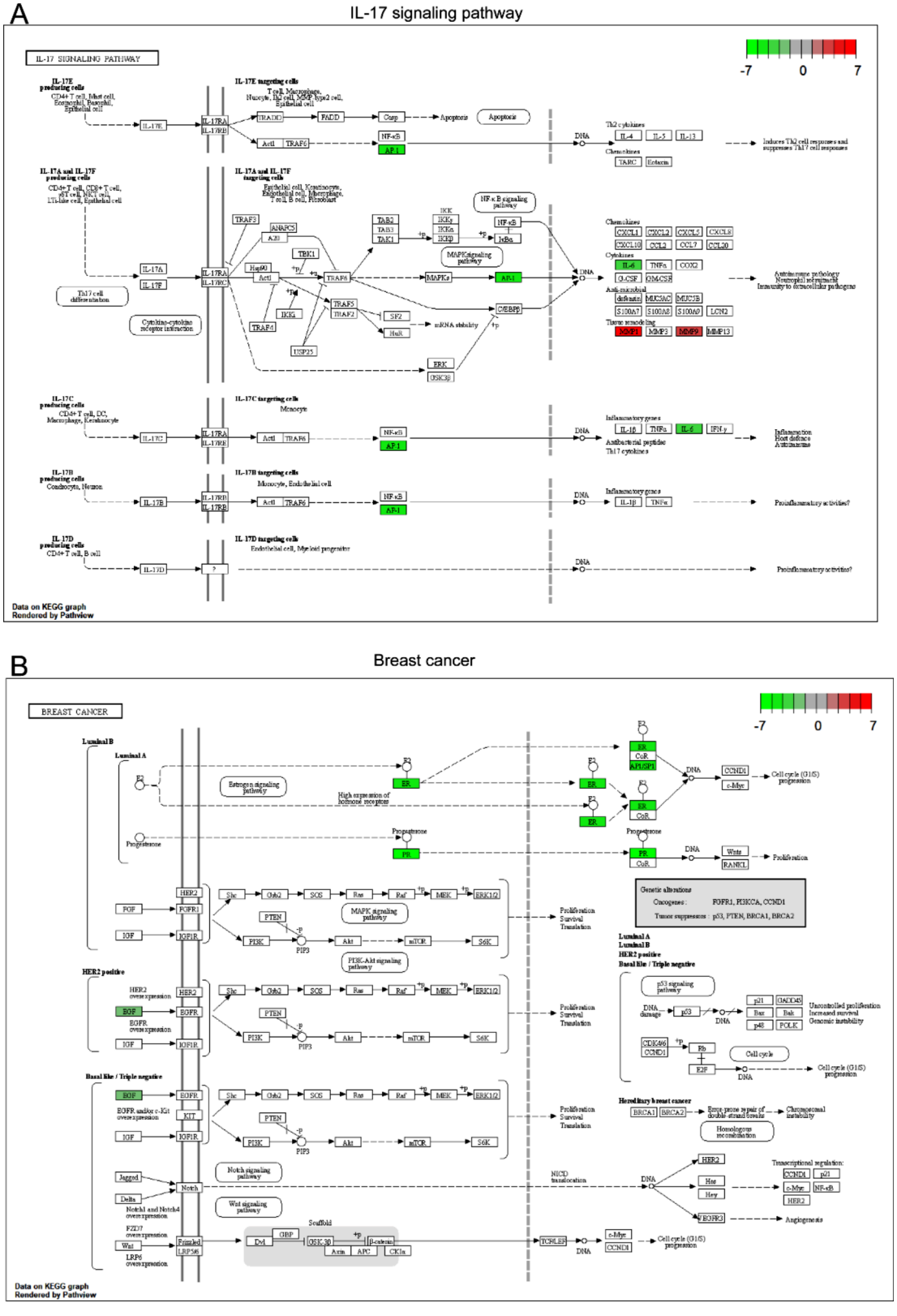

Fig. 6 KEGG enrichment analyses pathway plots. (**A**) IL-17 signaling pathway diagram. (**B**) Breast cancer pathway diagram. The color from green to red in A-B indicates the size of the logFC of hub genes. KEGG: Kyoto Encyclopedia of Genes and Genomes

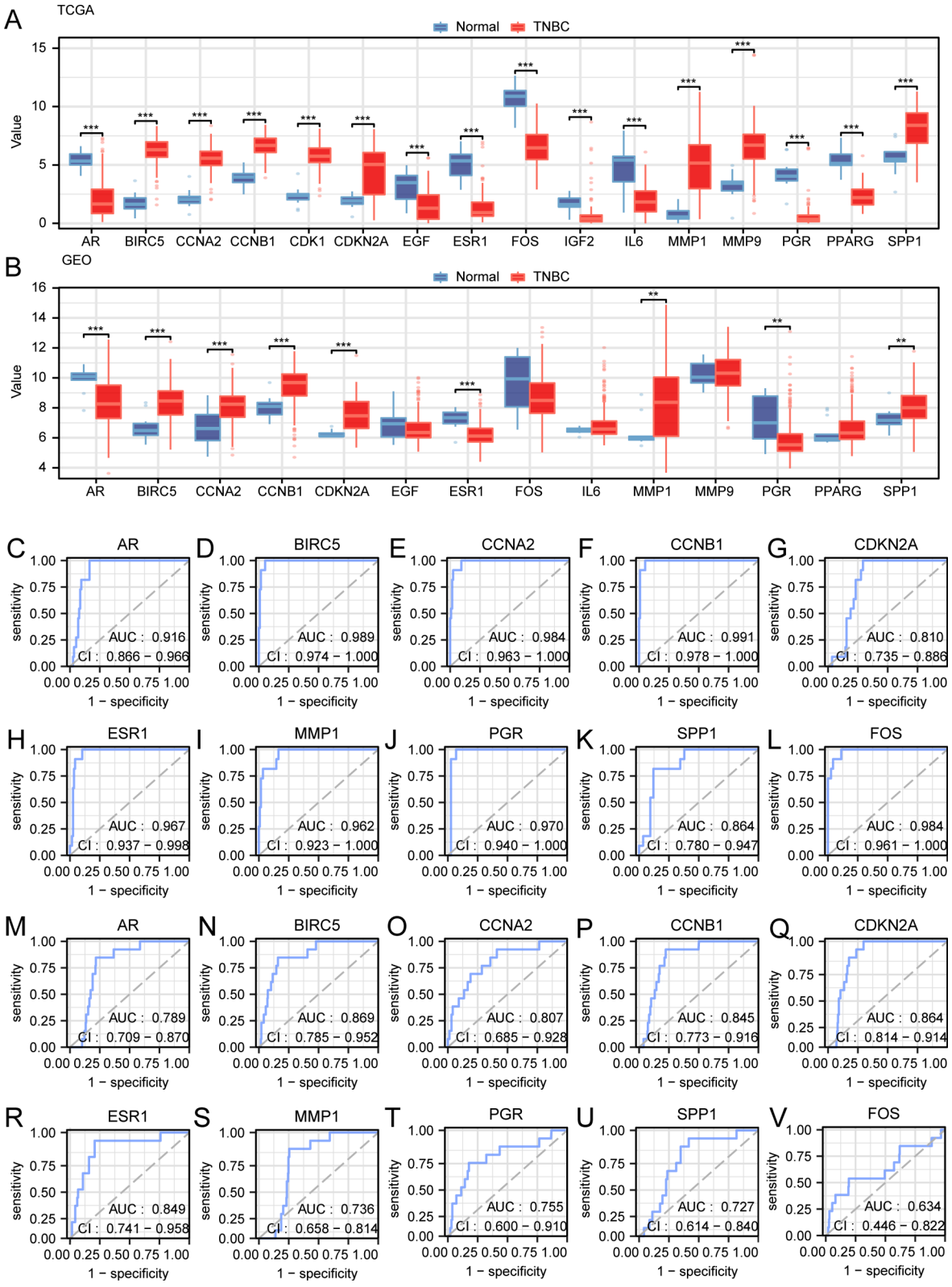

Fig. 7 Verification of the hub gene levels. (**A**-**B**) Comparison diagram showing the hub genes from different groups of TCGA-TNBC dataset (**A**) and the combined dataset (**B**) C-L. ROC verification of the hub genes from TCGA-TNBC dataset. M-V. ROC verification of the hub genes in the GEO-TNBC dataset. TNBC: Triple Negative Breast Cancer; ROC: receiver operating characteristic curve. * $p < 0.05$ signifies statistical significance; ** $p < 0.01$ signifies highly statistical significance; and *** $p < 0.001$ indicates extremely statistical significance. An AUC level approaching 1 suggests a superior diagnosis performance. AUC > 0.9 and 0.7–0.9 signifies a high and certain accuracy, respectively

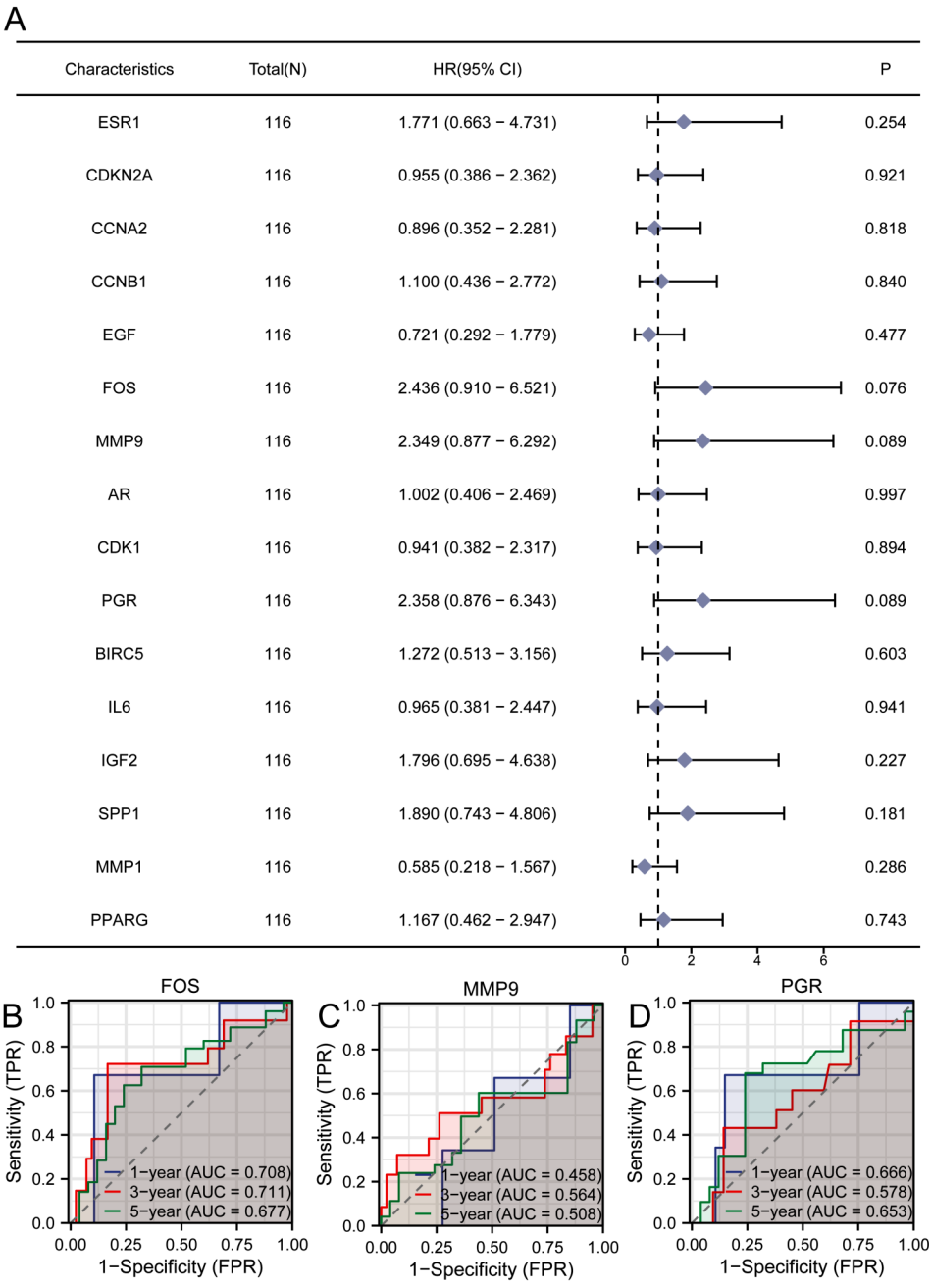

Fig. 8 Prognosis screening of the hub genes. (**A**) Forest map showing a univariate Cox analysis of the hub genes. (**B**-**D**) Time-dependent ROC analyses of *FOS* (**B**), *MMP9* (**C**), and *PGR* (**D**). An AUC value approaching 1 suggests a superior diagnosis performance. The AUCs of 0.5–0.7, 0.7–0.9, and > 0.9 signify low, partial, and high accuracy, respectively

Validation of the hub genes

To further validate the expression of the NRGs, RT-qPCR assays were performed on MDA-MB-468 human BC cells, MDA-MB-157 human BC cells, and MCF-10 A human breast epithelial cells. In the TNA subtype of TNBC cells (MDA-MB-468), the expression levels of *EGF* and *PPARG* were significantly elevated (Fig. 12A and D). In the TNB subtype of TNBC cells (MDA-MB-157), the expression levels of *PGR*, *PPARG*, and *IGF2* were significantly elevated (Fig. 12C, D, and E). Further, in the control group of normal human breast epithelial cells (MCF-10 A), the mRNA expression levels of *FOS*, *MMP1*, and *SPP1* were significantly increased (Fig. 12B, F, and G).

When we examined the mRNA expression of the hub genes in the model, we found that only the expression trend of *FOS* was consistent with the results of DEGs analyses, unlike the other hub genes. Therefore, *FOS* was

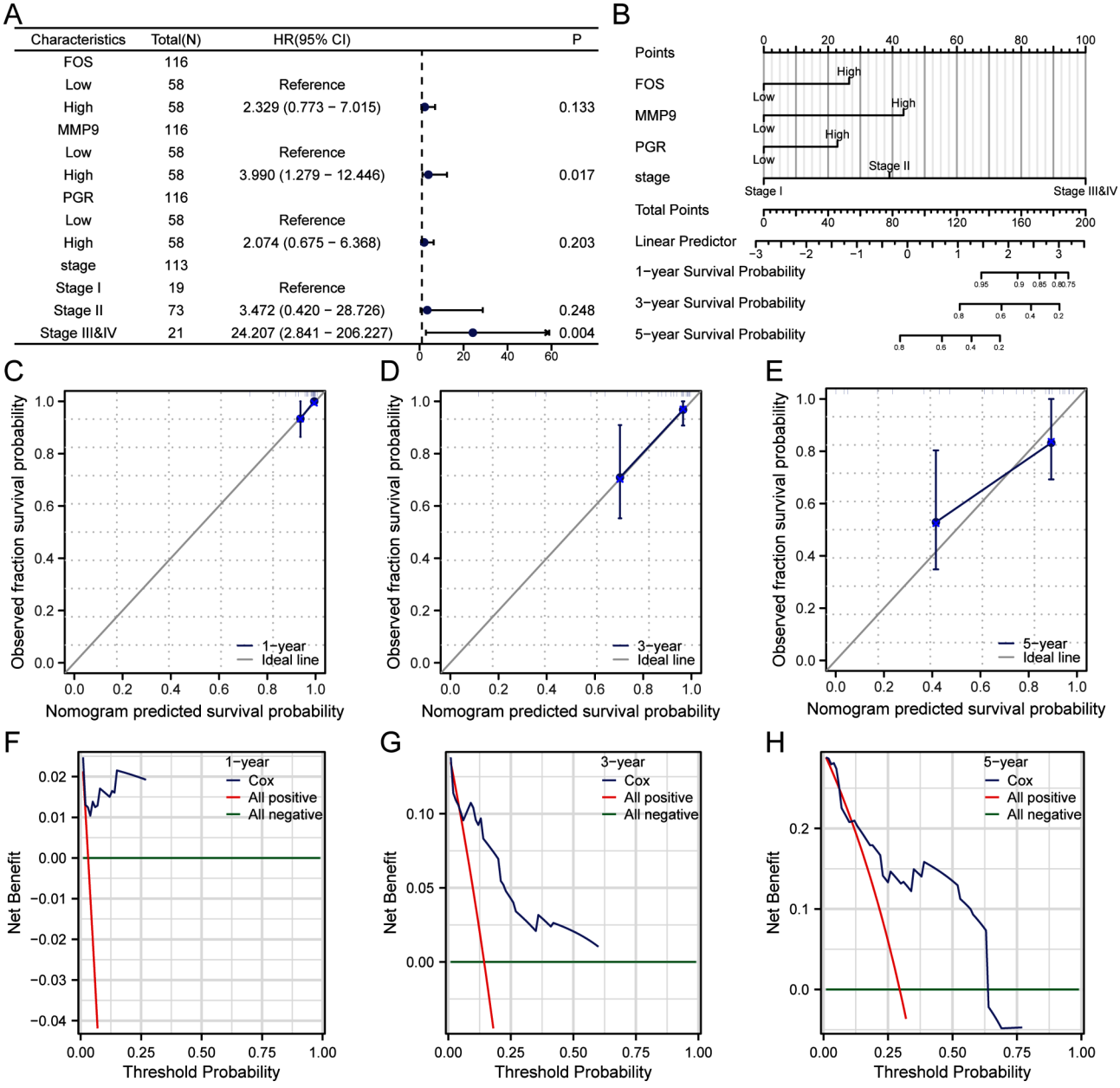

Fig. 9 Prognosis performance of the prognostic model. (**A**-**B**). Forest map (A) and nomogram (**B**) showing the multivariate Cox regression analysis. (**C**-**E**) 1- (**C**), 3- (**D**), and 5-year (**E**) calibration curve diagram in the nomogram analysis of the Cox regression prognostic model. (**F**-**H**) 1- (**F**), 3- (**G**), and 5-year (**H**) DCA diagram of the Cox regression prognostic model. DCA: Decision curve analysis

validated as the ultimate hub gene in the progression of TNBC.

Discussion

TNBC, a pathological subtype of BC with the highest malignancy grade, is characterized by poor differentiation, high invasiveness, easy metastasis, drug resistance, lack of effective target, limited therapeutic options, and a poor overall survival rate. At present, it remains challenging to treat TNBC; as a result, it is needed to search for therapeutic targets of TNBC, explore the therapeutics and associated molecular mechanisms, and prevent its recurrence and metastasis. HQSJZD is a classic decoction for tonifying qi, which mainly consists of Astragalus, Ginseng, Rhizoma Atractylodis, Poria cocos, and Glycyrrhiza. In recent years, HQSJZD has achieved favorable results in enhancing chemotherapeutic sensitivity of gastric cancer, increasing the radiotherapeutic efficiency in liver cancer patients, alleviating the side effects of chemotherapy for non-small cell lung cancer, and relieving fatigue symptoms in BC patients by regulating the immune system [39–43].Research concerning the effect

Table 3 Cox regression to identify the clinical features of TCGA-TNBC dataset

Characteristics	Total (*N*)	HR (95% CI) Univariate analysis	*P* value Univariate analysis	HR (95% CI) Multivariate analysis	*P* value Multivariate analysis
FOS	116		0.067		
Low	58	Reference		Reference	
High	58	2.436 (0.910–6.521)	0.076	2.329 (0.773–7.015)	0.133
MMP9	116		0.079		
Low	58	Reference		Reference	
High	58	2.349 (0.877–6.292)	0.089	3.990 (1.279–12.446)	0.017
PGR	116		0.079		
Low	58	Reference		Reference	
High	58	2.358 (0.876–6.343)	0.089	2.074 (0.675–6.368)	0.203
stage	113		< 0.001		
Stage I	19	Reference		Reference	
Stage II	73	2.899 (0.359–23.373)	0.318	3.472 (0.420–28.726)	0.248
Stage III&IV	21	16.789 (2.075–135.858)	0.008	24.207 (2.841–206.227)	0.004

of HQSJZD on the treatment of TNBC has been rarely reported. In the present study, the highly invasive and metastatic MDA-MB-231 and MDA-MB-468 TNBC cell lines were used to analyze the molecular mechanisms of HQSJZD in the treatment of TNBC. Besides, strict selection criteria were adopted to select the active ingredients of TCM from the TCMSP database and their potential targets were predicted. This approach improved the reliability and reproducibility of the results. Through bioinformatics analysis, we identified a series of differentially expressed genes (DEGs) and further screened out the hub genes related to HQSJZD, which provided directions for subsequent in-depth studies on their potential mechanisms of action in treating TNBC. Moreover, comprehensive validation and analysis of the hub genes were conducted. Also, the Wilcoxon rank-sum test was used to compare the expression of these genes among different groups (TNBC, Normal) in the TCGA-TNBC and combined GEO datasets. The ROC curves were plotted, which indicated that some hub genes showed high diagnostic value in different datasets (AUC>0.9). Besides, prognostic analysis was conducted to evaluate the prognostic value of hub genes through utilizing the univariate and multivariate Cox regression models. Particularly, FOS, MMP9, and PGR genes showed excellent performance in the 1-year, 3-year, and 5-year prediction. Further, immunoinfiltration analysis (CIBERSORT) revealed the infiltration of 22 immune cells in TNBC and showed significant correlations between some immune cells and hub genes, especially the close correlation of MMP9 with Macrophages M0. Pan-cancer analysis based on the TCGA database and human expression distribution analysis using the HPA database suggested the expression of prognosis-related hub genes (FOS, MMP9, and PGR) in various cancers and different human organs. FOS is a complex formed by nuclear phosphoproteins and the JUN/AP-1 transcription factor through the non-covalent bond tight junction, and its gene family is comprised of *c-FOS*, *FOSB*, *FOSL1*, and *FOSL2.* FOS is a regulatory factor for cell growth, transformation, and differentiation, and its gene expression is associated with cell apoptosis under certain specific circumstances [44]. Apigenin may inhibit the progression of hepatocellular carcinoma by suppressing the expression of *FOS*, *MAPK1*, and *miR-199a* [45].

In conclusion, this study indicates that FOS, MMP9, and PGR may play key roles in the progression and treatment of TNBC, and they are expected to become the novel therapeutic targets. By regulating the expression of these genes, new treatment methods may be provided for TNBC patients, finally improving the treatment efficacy and reducing the risk of recurrence and metastasis. For example, MMP9, as a key matrix metalloproteinase, promotes tumor cell invasion and metastasis by degrading the extracellular matrix; consequently, the inhibition of MMP9 may block the progression of TNBC [46]. Although PGR is typically lowly expressed in TNBC, the regulation of its activity in specific subtypes may provide new strategies for cancer treatment [47]. In addition, the low expression of the FOS gene may be associated with the invasiveness and migratory capacity of TNBC cells, and therefore, up-regulating FOS expression or activating its related pathways may suppress the malignant phenotype of TNBC [48]. Additionally, FOS, EGR1 and JUNB, are the key transcription factors in inflammatory BC [45]. As discovered in another study, the decreased *FOS* expression by teicoplanin promotes the growth and proliferation of BC cells [49]. Fos-related antigen-1 (FRA-1), belonging to the activator protein-1 (AP-1) transcription factor superfamily, is highly expressed in different cancer types like colon cancer, breast cancer, gastric cancer, lung cancer, and bladder cancer [50]. Therefore, as

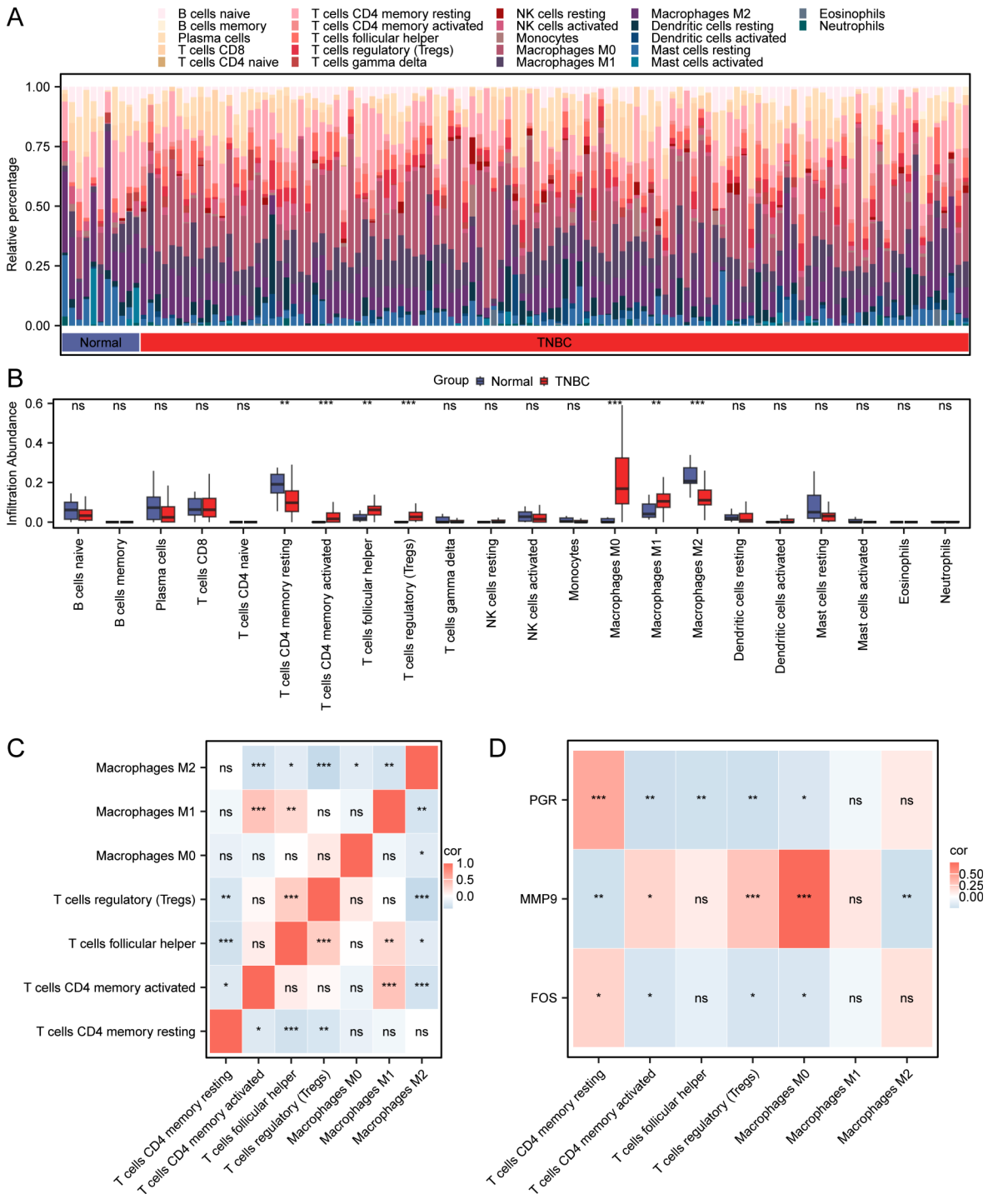

Fig. 10 Immune infiltration analyses (CIBERSORT). (**A**) Histogram showing the cumulative infiltration results of TCGA-TNBC dataset. (**B**) Comparison diagram showing immune cells of the different groups from TCGA-TNBC dataset. (**C**) Heat map showing the correlations among the immune cells. (**D**) Heat map displaying the correlations of the immune cells with the hub genes. ns represents no significance ($p \geq 0.05$); * $p < 0.05$ indicates statistical significance; ** $p < 0.01$ indicates highly statistical significance; and *** $p < 0.001$ indicates extremely statistical significance. TNBC: Triple Negative Breast Cancer

shown in this study, the *FOS* activity was tightly related to TNBC, and suppressing *FOS* expression could suppress the growth, migration, and invasion of TNBC cells. Finally, based on the RT-qPCR results, we found that the *FOS* core genes were differentially expressed in the MDA-MB-468 (TNA), MDA-MB-157 (TNB) and control groups, with low *FOS* expression in TNBC whereas high expression in normal breast epithelial cells. These

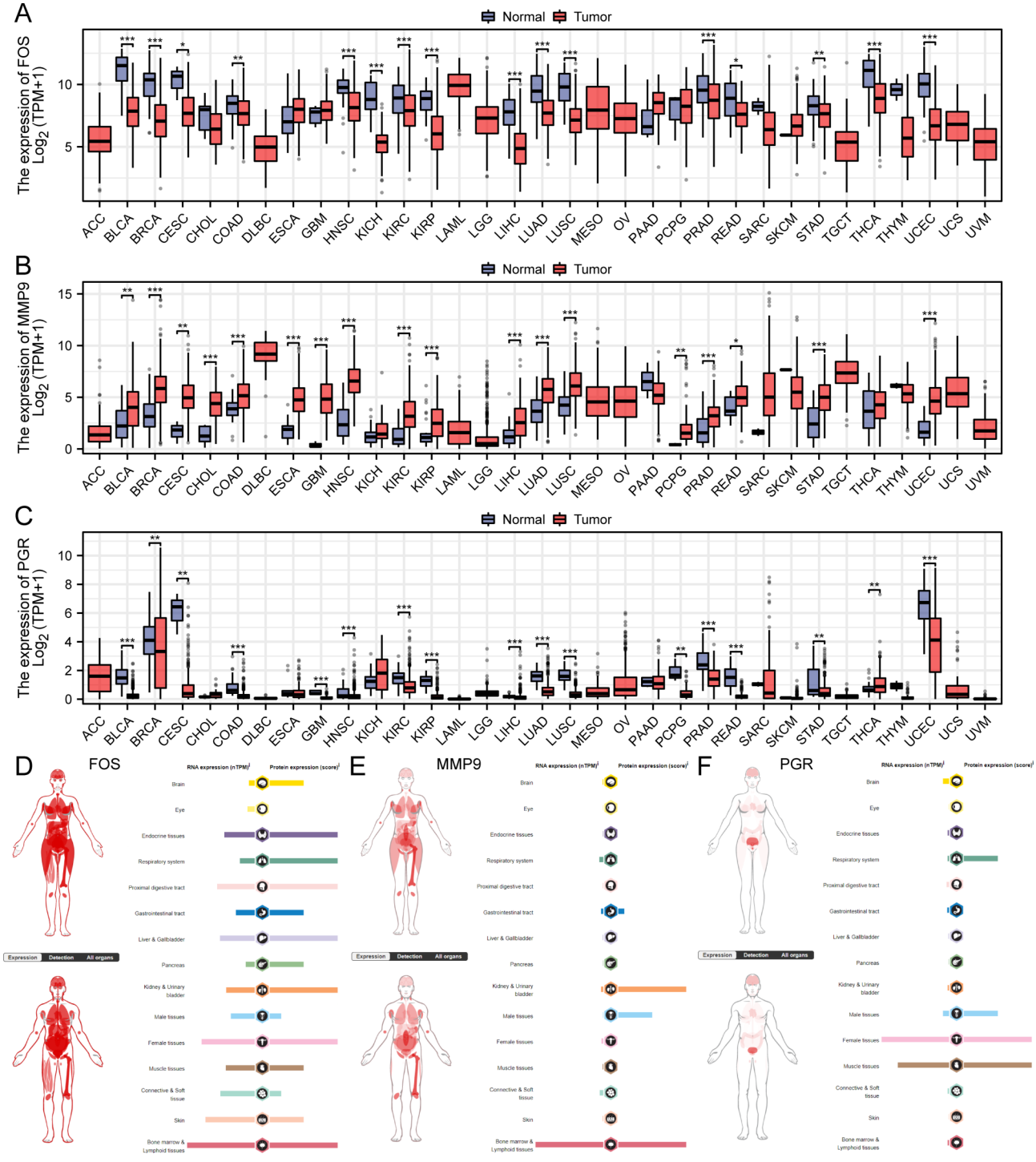

Fig. 11 Hub gene expression in pan-cancer and in the human body. **(A-C)**. Comparison diagram of *FOS* (**A**), MMP9 (**B**), and PGR (**C**) expression in pan-cancer. (**D-F**). *FOS* (**D**), *MMP9* (**E**), and *PGR* (**F**) expression in various human organs. * $p < 0.05$ signifies statistical significance; ** $p < 0.01$ signifies highly statistical significance; and *** $p < 0.001$ indicates extremely statistical significance

expression trends were consistent with previous bioinformatics analyses. Therefore, it is likely that TNBC can be treated through regulating the *FOS* gene. Moreover, we found that *FOS* had low expression in TNBC cells, while *FOS* overexpression was likely to inhibit the malignant phenotype of TNBC cells. Despite these important findings, the translation from experimental research to clinical practice still faces many challenges and limitations.

This study was designed to further clarify the signaling pathways and mechanisms of HQSJZD in treating TNBC.

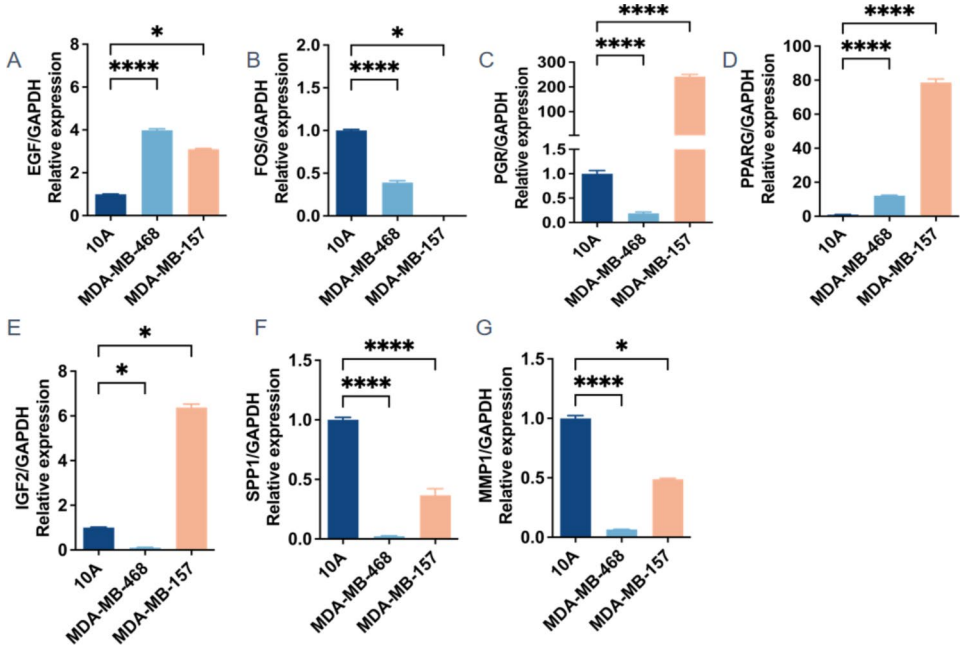

Fig. 12 The relative expression of the hub genes was determined by RT-qPCR. (**A**) EGF. (**B**) FOS. (**C**) PGR. (**D**) PPARG. (**E**) IGF2. (**F**) SPP1. (**G**) MMP1. *p<0.05,**p<0.01,***p<0.001,****p<0.0001

GO functional annotation determined that the CC terms such as cyclin-dependent protein kinase holoenzyme complex, transferase complex, protein kinase complex, transferring phosphorus-containing groups, and spindle, together with the hub genes might regulate BPs including epithelial cell proliferation and regulation of protein serine/threonine kinase activity for executing MFs like transcription coregulator binding, receptor ligand activity, and kinase regulator activity. In line with the KEGG analyses results, the hub genes were mostly associated with pathways such as the IL-17 pathway, cellular senescence, endocrine resistance, and BC. The IL-17 pathway represents the classical inflammation-related pathway, which mainly functions to induce and mediate pro-inflammatory responses and regulate multiple immune functions. Moreover, the heterodimer receptor complex, consisting of IL-17 and IL-17R receptor, can emit a signal to activate the downstream pathways like NF-kB, MAPKs, and C/EBPs, which can then promote antibacterial peptide, chemokine, and cytokine expression, thus triggering BPs including immune response, tumor genesis, and cell apoptosis [51]. The major mechanisms underlying the direct correlation between the IL-17 signaling pathway and the prognosis of BC include the direct action of tumor cells to promote tumor cell survival, invasion and migration; interaction with myeloid-derived suppressor cells (MDSCs) for suppressing anticancer immunity; and regulation of tumor angiogenesis [52–54]. As reported in some studies, IL-17 significantly enhances the invasiveness of the TNBC MDA-MB231 cell line, and such invasiveness can be suppressed by matrix metalloproteinase (MMP) [55]. Additionally, some studies demonstrate that dual-target drugs targeting the inflammatory (IL-17 A) and MMP pathways may be the new anticancer treatment, based on the notion that the interaction between IL-17 A and MMP-9 possibly accelerates tumor invasion and migration [56]. Consequently, the IL-17 signaling pathway is tightly associated with TNBC invasiveness, which may probably become the new therapeutic target of TNBC. Cellular senescence is the cellular status stimulated by pressure signals existing in a specific physiological process. The senescent cells can secrete various cytokines like growth factors, pro-inflammatory cytokines, and matrix remodeling enzymes and chemokines to promote the carcinogenesis of the adjacent pre-cancerous cells. These factors are of senescence-associated secretory phenotype (SASP) [57]. In tumor cells with PTEN deletion, SASP activates the JAK2/STAT3 pathway to form the immunosuppressive TME, thus promoting tumor progression [58]. Astragalus can induce cellular senescence to resist the activity of BC, and voluntarily and involuntarily suppresses tumor progression [58]. In addition, SASP up-regulates and releases pro-inflammatory factors (IL-6 and IL-1β), a proteinase (MMP3), and growth factors to remodel the TME and promote tumor development, distant metastasis, immune infiltration as well as the signaling pathways and regulatory mechanisms in overcoming resistance [59]. Collectively, HQS-JZD may exert its anti-TNBC effect by regulating cellular senescence, the IL-17 signaling pathway, and BC pathways via key targets.

The prognosis model constructed in this study innovatively proposed that FOS could serve as a new marker for TNBC, which has a high degree of malignancy and is currently a clinical challenge. Additionally, HQSJZD is likely to be a therapeutic agent targeting this marker. The present study provides new insights into the treatment of TNBC, and brings hope for patients with this aggressive disease. Regardless of the valuable insights provided in this study, there are still several limitations that need to be overcome and improved in future research. For instance, the main database used for predicting the active ingredients and targets of TCM in this study was TCMSP. While TCMSP is a widely used authoritative database, due to limitations of a single database, some potential targets may not be identified. Besides, the limited sample size may affect the universality and representativeness of the results. The experimental validation part of this study used a limited number of cell lines (MDA-MB-468, MDA-MB-157, and MCF-10 A). Therefore, future research should expand the sample size to include more different types of TNBC cell lines and patient samples, so as to verify and support our findings. Additionally, used the RT-qPCR method was utilized in this study to validate the expression of hub genes. Although RT-qPCR is a reliable quantitative method, a single validation method may not be sufficient to fully reveal the roles of these genes in the disease. In this regard, future research should combine protein-level validation (such as Western blot) and functional experiments (including gene knockout and overexpression experiments) to more comprehensively validate our results. Further, the experiments in this study were mainly conducted using the in vitro cell models. Although cell experiments provide valuable preliminary data, there are differences between in vitro environments and in vivo environments. So subsequent research should include animal model experiments, and even clinical sample studies, for the sake of better understanding the actual effects and mechanisms of HQSJZD in the treatment of TNBC.

Supplementary Information

The online version contains supplementary material available at https://doi.org/10.1186/s12885-024-12957-5.

Supplementary Material 1

Supplementary Material 2

Supplementary Material 3

Supplementary Material 4

Author contributions

Yixin Cui, Yin Zhang and Decai Wang designed research; Haiming Wang analyzed data; Jiwei MI was in charge of doing the experiment; Decai Wang, Shuai Meng, Haiming Wang and Lingsheng Li performed research; Decai Wang, Jiwei MI and Yixin Cui wrote the paper; Dongqing Xie collected the public data and repeatedly proofread, translated and polished the language of the articles. All authors reviewed the manuscript.

Funding

Not applicable.

Data availability

Data are available in a public, open access repository, Data are available on reasonable request. All data relevant to the study are included in the article or uploaded as supplemental information, The datasets (GEO data) and (TCGA LIHC data) and (TCMSP database) for this study carbe found in the GEO (https://www.ncbi.nlm.nih.gov/) and TCGA (TCGA, The cancer genome atlas, https://portal.gdc.cancer.gov/) and TCMSP database (https://tcmspw.com/tcmsp.php.

Declarations

Ethical approval

The study was conducted using established cell lines exclusively. No human or animal subjects were involved in this research. Therefore, ethical approval from an Institutional Review Board (IRB) or Ethics Committee was not required.All cell lines used in this study were obtained from reliable and certified sources, and were handled in accordance with institutional guidelines and regulations. The authors declare no ethical conflicts associated with this research.

Conflict of interest

The authors declare no conflict of interest.

Author details

[1]Aerospace Center Hospital, Beijing 100049, China
[2]Ultrasound Diagnosis Department, The First Medical Center of PLA General Hospital, Beijing 100853, China
[3]Department of Traditional Chinese Medicine, The Sixth Medical Center of PLA General Hospital, Beijing 100048, China
[4]Department of Neurology, The Central People's Hospital, Zhanjiang, Guangdong 524037, China

Received: 23 April 2024 / Accepted: 17 September 2024
Published online: 30 September 2024

References

1. Latest Interpretation of Global Cancer. Statistics in 2020 [J]. Chin Oncol Clin Rehabilitation. 2021;28(03):301.
2. Abbed T, Shifrin DA. Aesthetic female -to -male chest Transformation: power of combining modified mastectomy with a Pectoral Implant [J]. Plast Reconstr Surg Global Open. 2017;5(8):e1445.
3. Lv Zhijian C, Yugen L. Correlation of clinicopathological features with prognosis of triple-negative breast cancer patients of different age groups [J]. J Clin Surg. 2020;28(03):250–3.
4. Oshi Masanori K, Tsutomu Y, Li P, Xuan Q, Qianya T, Wanqing S, Amy MD, KerryAnn N, Sumana Y, Jessica L, Song ML, Gt C, Timothy A, Kalinski, Pawel. Matsuyama Ryusei, Otsuji Eigo, Endo Itaru, Takabe Kazuaki. Immune cytolytic activity is associated with reduced intra-tumoral genetic heterogeneity and with better clinical outcomes in triple negative breast cancer [J]. Am J cancer Res, 2021;11(7).
5. Wang Zheng W, Hui S, Xi F, Shu-Ning YLS-SD. Chen Xiao-Song, Shen Kun-Wei. A risk stratification model for Predicting overall survival and Surgical Benefit in Triple-negative breast Cancer patients with de novo distant metastasis [J]. Front Oncol. 2020;10(10).
6. Li X, Xingyong S, Zhen H. Therapeutic effect of Oxaliplatin combined with Tegafur Gimeracil Oteracil Potassium Capsule in treating metastatic or non-resectable locally advanced triple negative breast cancer [J]. Chin Oncol Clin Rehabilitation. 2020;27(11):1294–7.
7. Li H, Wei L, Jianqiang S. Wang Zunyi. Changes in blood-derived exosomal Mi RNA-27a/P-gp in triple negative breast cancer patients after neoadjuvant chemotherapy and the influence on angiogenesis [J]. J Xuzhou Med Univ. 2021;(05):357–62.

8. Zhang F, Zhuo Z, Lijuan Z, Wei X. Radiotherapy of early triple negative breast cancer after modified radical mastectomy and the prognosis-related factor analysis [J]. Chin J Radiological Med Prot. 2018;(07):510–6.
9. Jian HX-CZ, Bing-He X, et al. Cisplatin plus gemcitabine versus paclitaxel plus gemcitabine as first-line therapy for metastatic triple-negative breast cancer (CBCSG006): a randomised, open-label, multicentre, phase 3 trial [J]. Lancet Oncol. 2015;16:436–46.
10. Xie Rongdan. The suppression of Astragalus polysaccharides on the xenograft tumor growth in nude mice implanted with triple negative breast cancer MDA-MB-231 cells [D]. Tumor: Long Feng. Gansu University of Traditional Chinese Medicine; 2019.
11. Zhang Daidi. Suppression of Sijunzi decoction extract on the growth of human triple negative breast cancer MDA-MB-468 cells [D]. Tutor: Li Duolu. Zhengzhou University; 2020.
12. Xu Xudong C, Gang Y, Bo YJ. Effect of Astragalus Sijunzi decoction combined with early enteral nutrition on postoperative recovery for esophageal cancer [J]. Zhejiang J Integr Traditional Chin Western Med. 2012;(11):859–60.
13. Fu Yuewu F, Yanhong C, Rong T, Zhijian C. Zhiqiang. Astragalus Sijunzi decoction combined with parenteral nutrition promotes the postoperative recovery of gastric cancer patients [J]. J Guangzhou Univ Chin Med. 2007;(06):459–61.
14. Li X, Dequan Y, Changyi L, Xueyuan H. Effect of Astragalus Sijunzi decoction on the radiosensitivity and immune function of senile patients with primary liver cancer receiving radiotherapy [J]. Chin J Gerontol. 2019;(16):3937–40.
15. Chen Junlin Z, Yitian, Dajun Y. Exploring the mechanism of Huangqi Sijunzi Decoction in the Treatment of Hepatocellular Carcinoma Based on Network Pharmacology and Bioinformatics [J]. J Zhejiang Univ Traditional Chin Med. 2023;47(12):1395–405.
16. Liu Haopeng. Research on the Effect of Huangqi Simianqincao Decoction in Postoperative Chemotherapy patients with breast Cancer [D]. Mentor: Han Jie. Jining Medical College; 2023.
17. Cui Yixin M, Jiwei F, Linsheng YL, Yujia W, Jian H. Efficacy and mechanism of Astragalus gentleman decoction in the treatment of breast cancer fatigue: based on 94 clinical randomized controlled trials and network pharmacology [J]. J South Med Univ. 2022;42(05):649–57.
18. Ru J, Li P, Wang J, Zhou W, Li B, Huang C, Li P, Guo Z, Tao W, Yang Y, Xu X, Li Y, Wang Y, Yang L. TCMSP: a database of systems pharmacology for drug discovery from herbal medicines. J Cheminform. 2014;6:13.
19. Colaprico A, et al. TCGAbiolinks: an R/Bioconductor package for integrative analysis of TCGA data. Nucleic Acids Res. 2016;44(8):e71.
20. Goldman MJ, et al. Visualizing and interpreting cancer genomics data via the Xena platform. Nat Biotechnol. 2020;38(6):675–8.
21. Komatsu M, et al. Molecular features of triple negative breast cancer cells by genome-wide gene expression profiling analysis. Int J Oncol. 2013;42(2):478–506.
22. Burstein MD, et al. Comprehensive genomic analysis identifies novel subtypes and targets of triple-negative breast cancer. Clin Cancer Res. 2015;21(7):1688–98.
23. Davis S, Meltzer PS. GEOquery: a bridge between the Gene expression Omnibus (GEO) and BioConductor. Bioinformatics. 2007;23(14):1846–7.
24. Szklarczyk D, et al. STRING v11: protein-protein association networks with increased coverage, supporting functional discovery in genome-wide experimental datasets. Nucleic Acids Res. 2019;47(D1):D607–13.
25. Shannon P, et al. Cytoscape: a software environment for integrated models of biomolecular interaction networks. Genome Res. 2003;13(11):2498–504.
26. Chin CH, et al. cytoHubba: identifying hub objects and sub-networks from complex interactome. BMC Syst Biol. 2014;8(Suppl 4):S11.
27. Yu G. Gene ontology semantic similarity analysis using GOSemSim. Methods Mol Biol. 2020;2117:207–15.
28. Yu G, et al. clusterProfiler: an R package for comparing biological themes among gene clusters. Omics. 2012;16(5):284–7.
29. Luo W, Brouwer C. Pathview: an R/Bioconductor package for pathway-based data integration and visualization. Bioinformatics. 2013;29(14):1830–1.
30. Kanehisa M, Goto S. KEGG: kyoto encyclopedia of genes and genomes. Nucleic Acids Res. 2000;28(1):27–30.
31. Leek JT, et al. The sva package for removing batch effects and other unwanted variation in high-throughput experiments. Bioinformatics. 2012;28(6):882–3.
32. Park SY. Nomogram: an analogue tool to deliver digital knowledge. J Thorac Cardiovasc Surg. 2018;155(4):1793.
33. Perkins NJ, et al. Combining biomarker Calibration Data to Reduce Measurement Error. Epidemiology. 2019;30(Suppl 2):S3–9.
34. Van Calster B, et al. Reporting and interpreting decision curve analysis: a guide for investigators. Eur Urol. 2018;74(6):796–804.
35. Tataranni T, Piccoli C. Dichloroacetate (DCA) and Cancer: An Overview towards Clinical Applications. Oxid Med Cell Longev. 2019; 2019: 8201079.
36. Newman AM et al. Determining cell type abundance and expression from bulk tissues with digital cytometry. 2019;37(7):773–82.
37. Thul PJ, Lindskog C. The human protein atlas: a spatial map of the human proteome. Protein Sci. 2018;27(1):233–44.
38. Cheon K, Jaesuk K, Ju YD. Suppression of metastasis through inhibition of chitinase 3-like 1 expression by miR-125a-3p-mediated up-regulation of USF1 [J]. Theranostics. 2018;8:0.
39. Zhu Huiyan S, Hejuan, Wang Y. Effect of Huangqi Sijunzi decoction on postoperative recovery and immune function of patients with primary liver cancer [J]. Liaoning J Traditional Chin Med. 1–9.
40. Xie Guiping H, Yani Z, Jing Y, Xuequan, Shen Lizong. Clinical study of Huangqi Sijunzi Decoction on sensitivities of adjuvant chemotherapy for advanced gastric cancer [J]. Chin J Traditional Chin Med. 2022;(03):1810–4.
41. Tang Yale HT. Effects of Huangqi Sijunzi Decoction on Immune function of advanced primary liver cancer with Qi and blood deficiency [J]. J Practical Chin Med Intern Med. 2021;(09):20–2.
42. Xie GP. The preliminary study of Huangqi Sijunzi Decoction enhancing preoperative adjuvant chemotherapy sensitivity and related mechanism for advanced gastric cancer [D]. Tutor: Shen Lizong. Nanjing University of Traditional Chinese Medicine; 2021.
43. Ding Jiji M, Zhaolin. Application of Huangqi Sijunzi Decoction in chemotherapy of advanced non-small cell lung cancer [J]. Zhejiang J Integr Traditional Western Med. 2006;(01):28–9.
44. Safran M, Dalah I, Alexander J, Rosen N, Iny Stein T, Shmoish M, Nativ N, Bahir I, Doniger T, Krug H, Sirota-Madi A, Olender T, Golan Y, Stelzer G, Harel A, Lancet D. GeneCards Version 3: the human gene integrator. Database: J Biol Databases Curation. 2010;2010:baq020.
45. Wang S-M. Zhang Shu-Hui. Apigenin inhibits the growth of Hepatocellular Carcinoma Cells by affecting the expression of microRNA transcriptome. Front Oncol. 2021;11(undefined):657665. https://doi.org/10.3389/fonc.2021.657665.
46. Lakisha D, Moore-Smith I, Tatyana LJ, Hyoung, et al. Silencing of TGF-β1 in tumor cells impacts MMP-9 in tumor microenvironment [J]. Sci Rep. 2017;7(1):8678.
47. Muhammad S, Peng Z, Muhammad W, Guojun Z, Yousef A, Gezahign BJ. Mohammed, Bouhrhia. Targeting human progesterone receptor (PR), through pharmacophore-based screening and molecular simulation revealed potent inhibitors against breast cancer. Sci Rep. 2024;14(1):0. https://doi.org/10.1038/s41598-024-55321-0.
48. Song J-H, Byungdoo H, Sung LP, Hoon K, Soontag J, Changsun C. Myung Lee Hwan, Yun Seok-Joong, Hyun Choi Yung, Cha Eun-Jong, Patterson Cam, Kim Wun-Jae, Moon Sung-Kwon. IL-28A/IL-10Rβ axis promotes angiogenesis via eNOS/AKT signaling and AP-1/NF-κB/MMP-2 network by regulating HSP70-1 expression. J Adv Res. 2024;0(0):0. https://doi.org/10.1016/j.jare.2024.08.013
49. Ashouri Saeideh KM, Hosseindokht K, Mohammad K, Majid. Effect of teicoplanin on the expression of c-myc and c-*FOS* proto-oncogenes in MCF-7 breast cancer cell line. Adv Biomed Res. 2016;5(undefined). https://doi.org/10.4103/2277-9175.190984.
50. Feng Z, Junyu H, Xi J, et al. FRA-1: a key factor regulating signal transduction of tumor cells and a potential target molecule for tumor therapy [J]. Biomed Pharmacother. 2022;150:0.
51. Xu Z. Preparation of anti-human interleukin-17RA monoclonal antibody and its activity research [D]. Peking Union Medical College; 2016.
52. Chi-Cheng TY-FH, Yen-Shu L, et al. Interleukin 17A promotes cell migration, enhances anoikis resistance, and creates a microenvironment suitable for triple negative breast cancer tumor metastasis [J]. Cancer Immunol Immunother. 2021;70:2339–51.
53. Dawod Bassel L, Jinghua G, Simon, et al. Myeloid-derived suppressor cell depletion therapy targets IL-17A-expressing mammary carcinomas [J]. Sci Rep. 2020;10:13343.
54. Peng QX-LX, Yi-Qian Z, et al. Increased number of intratumoral IL-17 + cells, a harbinger of the adverse prognosis of triple-negative breast cancer [J]. Breast Cancer Res Treat. 2020;180:311–9.
55. Zhu XingWu, Mulcahy Lori A, Mohammed Rabab A, et al. IL-17 expression by breast-cancer-associated macrophages: IL-17 promotes invasiveness of breast cancer cell lines [J]. Breast Cancer Res. 2008;10:R95.

56. Koslawsky Dana Z, Marianna A, Ron, et al. A bi-specific inhibitor targeting IL-17A and MMP-9 reduces invasion and motility in MDA-MB-231 cells [J]. Oncotarget. 2018;9:28500–13.
57. Coppe JP, Patil CK, Rodier F, et al. Senescence-associated secretory phenotypes reveal cell-nonautonomous functions of oncogenic RAS and the p53 tumor suppressor [J]. PLoS Biol. 2008;6(12):2853–68.
58. Toso A, Revandkar A, Mitri D, et al. Enhancing chemotherapy efficacy in Pten-deficient prostate tumors by activating the senescence-associated antitumor immunity [J]. Cell Rep. 2014;9(1):75–89. https://doi.org/10.1016/j.celrep.2014.08.044.
59. Yang Dawei,Guo Qinglong,Liang Yin. Wogonin induces cellular senescence in breast cancer via suppressing TXNRD2 expression [J]. Arch Toxicol. 2020;94.

Publisher's note

Springer Nature remains neutral with regard to jurisdictional claims in published maps and institutional affiliations.